WRES: a novel 3DoF WRist ExoSkeleton with tendon-driven differential transmission for neuro-rehabilitation and teleoperation

Domenico Buongiorno[1], Edoardo Sotgiu[1,2], Daniele Leonardis[1], Simone Marcheschi[1], Massimiliano Solazzi[1] and Antonio Frisoli[1]

Abstract—In this paper the authors proposed a new wrist exoskeleton designed to provide kinesthetic feedback to the wrist user' joints for rehabilitative, teleoperation and virtual environment interaction purposes. The design process focused on the need to use the interface as the end-effector of a whole bimanual upper limb exoskeleton system, composed of two exoskeleton arms with seven degrees of freedom (DoF) each and two hand exoskeletons for all the fingers. The guideline of the design pointed to reach a trade-off between high transparency and low weight. In addition, both the compactness and mass distribution have played an important role in the design process due to the need to perform bimanual task and interaction. The proposed device was designed adopting a tendon-cable transmission for all the three joints. A differential transmission solution has been adopted to actuate the flexion/extension and radial/ulnar deviation joints, which allows to achieve lower inertia and higher compactness than a serial transmission. A first prototype has been build and characterized with several experimental tests showing its suitability for both teleoperation and rehabilitative therapy. Finally, the wrist device has been integrated with both the arm and the hand exoskeleton to prove the requirement observance.

Index Terms—Prosthetics and Exoskeletons; Tendon/Wire Mechanism; Haptics and Haptic Interfaces; Rehabilitation Robotics; Telerobotics and Teleoperation.

I. INTRODUCTION

IN the last decade, the exploding need of both higher immersivity in physical virtual environment interaction and more advanced robotic interfaces has pushed the scientific community to find new solutions for more complex robotic interfaces able to interact with the humans. Such a trend is explained by the growing interest in virtual environment physical interaction and robot-aided neuro-rehabilitation. In this scenario, exoskeletons represent an important component of telexistence cockpits [1] and innovative neuro-rehabilitation systems [2], [3]. An exoskeleton is a robotic device that can be worn on the user's body, representing the system with the highest physical symbiosis with the human operator.

In this work we present the design and experimental evaluation of a new three DoF wrist exoskeleton, the WRES.
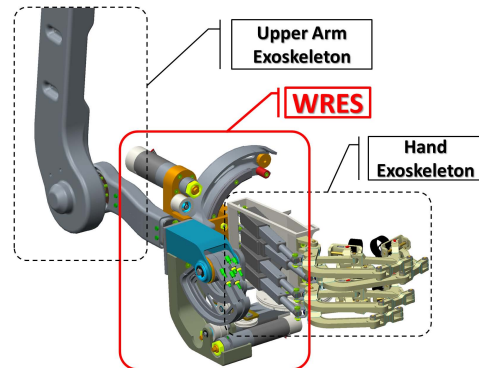
Fig. 1: Basic configuration of the WRES interface with Hand exoskeleton interface, mounted on exoskeleton upper arm.

The WRES is an active three Dofs wrist exoskeleton with a spherical serial kinematics and based on tendon transmissions. The rationale behind this work is the design of a fully actuated bimanual upper limb exoskeleton system, as shown in Fig. 1 and Fig. 12. The whole system is devised to have two robotic arms exoskeleton with seven DoFs each (three for the shoulder articulation, one for the elbow joint and three for the wrist articulation) and two fully actuated hand exoskeletons. At SSSA premises both a bilateral arm exoskeleton (ALEx - Arm Light Exoskeleton) [4] with the first 4 DoF (shoulder, elbow) and a new hand exoskeleton [5] have been already designed and evaluated. The new WRES wrist exoskeleton has been devised so to complete the fully actuated exoskeleton, and to this aim has to fulfill several requirements: (a) to be low-weight, in order to be mounted on the top of the ALEx exoskeleton; (b) to be able to accommodate the hand exoskeleton at its end-effector; (c) to be characterized by an optimal weight/actuation torques ratio; (d) to be compact with an optimal mass distribution allowing bimanual tasks, i.e. manipulation of small virtual or real objects.

The WRES presented design (Fig. 3) introduces a novel capstan-based tendon driven solution to actuate a differential transmission. To the authors' knowledge, for the first time a differential transmission is designed with the encumbrance completely distributed on only one side. In the particular application of this paper, the differential transmission is used to actuate the flexion/extension (FE) and radial/ulnar (RU) deviation joints. Such a novel cabled transmission allows the last two actuators to be placed closer to the base so reducing

the moving mass compared to a serial structure.

Thanks to the optimal mass distribution, that is completely on the dorsal side of the human hand, the hand palm is free allowing bimanual task interaction with virtual and real objects. To ensure a high backdrivability, the first prono-supination joint is actuated with a tendon transmission, too. Since the rationale of the work is the development of a fully actuated bimanual upper limb exoskeleton, the design process took into account the mass distribution on the internal part of the forearm to avoid interferences between two worn wrist exoskeletons. The developed exoskeleton can be also mounted on a arm exoskeleton due to its high compactness and its low weight; in this particular work it has been mounted on the ALEx exoskeleton end-effector. Finally, to observe all the requirements, it can accommodate the PERCRO hand exoskeleton. Since ALEx exoskeleton is a grounded device, the weight of the WRES, of the hand exoskeleton, and of the ALEx's links is entirely compensated by the system. Then, all the resulting reaction forces and torques are transmitted to the ALEx base frame without affecting the user.

In the sections that follow, we present an overview of the state of the art, then the design and controller development, with details on the mechanical design and the actuation part first and the electronics, the low level control and friction compensation later. Finally, we present the results of the system identification and from testing experiments to evaluate its transparency and its capacity in haptic tasks.

II. SURVEY OF EXISTING LITERATURE

Several exoskeleton devices for upper limb interaction have been presented in the last years ([3]). Only few of them have more than four actuated DoFs necessary for the main upper limb articulations [6], [7], [8]. The CADEN 7 ([6]) is cable-actuated dexterous exoskeleton with seven actuated DoFs (four for the shoulder, one for the elbow and three for wrist). Both the ARMIN III ([7]) and HARMONY ([8]) have six actuated DoFs (four for the shoulder, one for the elbow and two for wrist). To the authors' knowledge a seven actuated DoFs upper limb exoskeleton with a fully actuated hand exoskeleton has not yet been presented. In addition to upper limb exoskeletons that might include some or all the wrist DoFs, several independent wrist robotic devices have
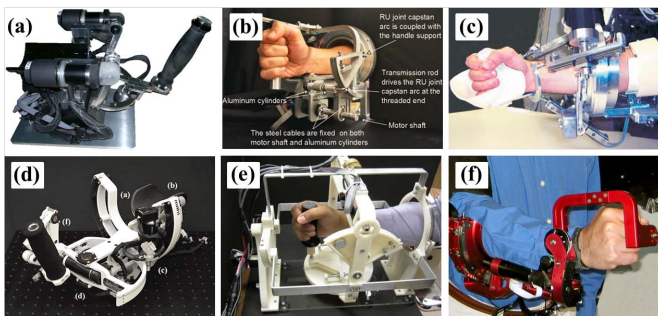
been presented so far ([9], [10], [11], [12], [13], [6]). As depicted in Fig. 2, the wrist exoskeleton solutions in literature are based on different approaches concerning the kinematics, the mechanics and the power transmission. The Wrist-Robot [9], shown in Fig. 2a, has the high back-drivability of the 3 DoFs as main requirement. The mechanical solution is based on a serial kinematics actuated by gearmotors; in particular the RU joint is actuated by two parallel coupled motors. The RiceWrist-S, reported in Fig. 2b, is cable-driven serial mechanism actuated by DC motors. Sergi, in [11], proposed a wrist robotic device (shown in Fig. 2c) based on a parallel structure and powered by linear series elastic actuators purposely designed for safety interaction. The high physical compliance guaranteed by this device comes at the expense of high encumbrance and difficulty to be don/doff.

Like the RiceWrist-S, the OpenWrist, shown in Fig. 2d, employs a serial RRR mechanism for manipulation of the users wrist. Power is transmitted through capstan-cable drives. Several improvements and new features were implemented with respect to the precedent prototypes: polymer-ceramic coating, easiness in changing hand-side configuration, passive DoF to compensate axis misalignment, high performance and a simple don/doff procedure. The Wrist Gimbal, shown in Fig. 2e, is a three DoFs exoskeleton characterized by a high mechanical rigidity thanks to its parallel structure. The wrist module of the Caden 7 exoskeleton, reported in Fig. 2f, is an impedance-based wrist exoskeleton. It has three DoFs driven by a tendon-based transmission.

All the devices described above are not suitable for our purpose since they do not respect all the imposed requirements. Even though the solutions shown in Fig. 2a,b,c,d could accommodate the hand exoskeleton and could be mounted at the end-effector of an upper arm exoskeleton, the encumbrance of the fixed and moving parts doesn't allow their use in bimanual tasks. In fact, mounting any of the devices shown in Fig. 2a,b,c,d on two arm exoskeletons, some parts might interfere each other or with the opposite hand exoskeleton and human

Fig. 2: **Existing 3 DoFs wrist exoskeleton.** Figures (a), (b), (b), (d), (e) and (f) show the wrist exoskeletons presented in [9], [10], [11], [12], [13], and [6], respectively.
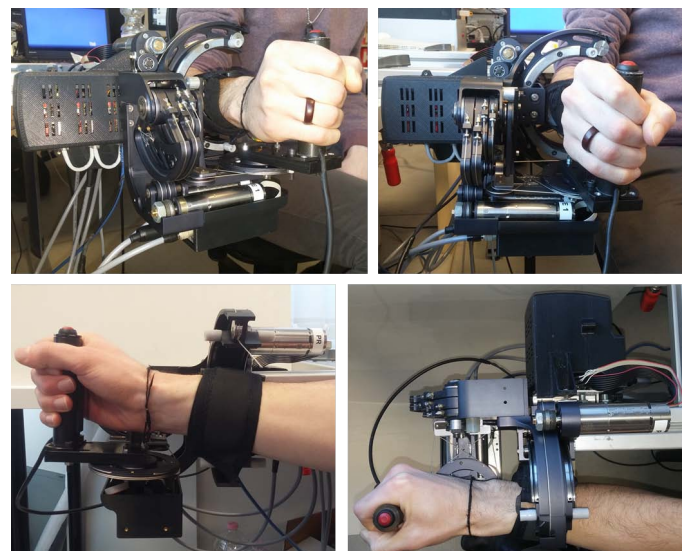
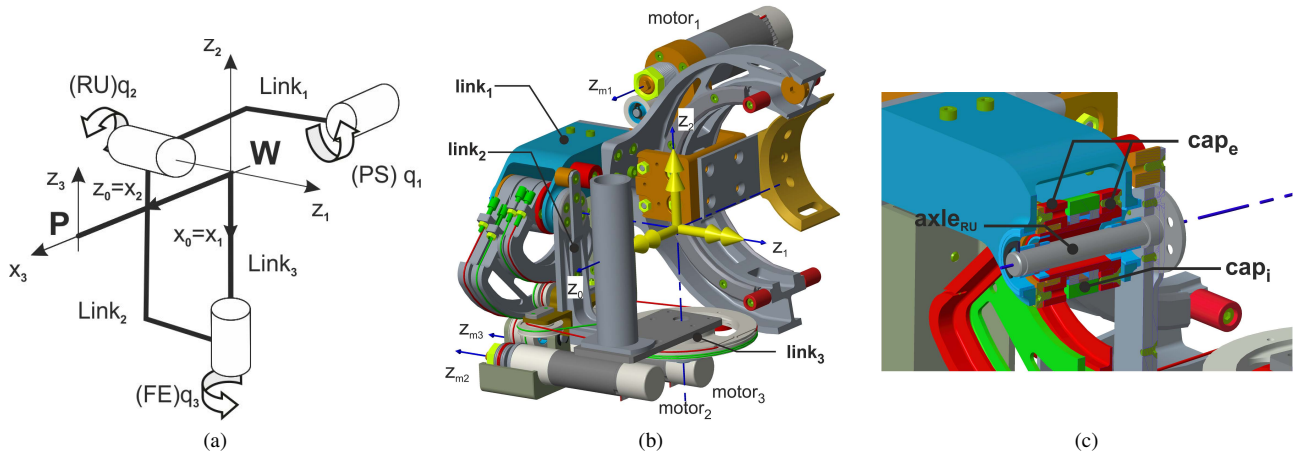

Fig. 3: WRES device worn by a user.

Fig. 4: The schematic representation of wrist device kinematics is depicted in (a); the device's CAD model is shown in (b). The section from the CAD model, in (c), shows the mechanical solution adopted to allow that the four capstans were mounted on the same side with respect to the $z_0 - z_2$ plane. The hollow shaft, which insists on the main RU axle through a couple of steel ball bearings, yokes both the external capstans (in red). At the same time, the hollow shaft supports the internal capstans pair (in green) through a couple of thin steel ball bearings.

arm. Since these four exoskeletons have been thought as grounded devices, they present a significant mass distribution in the bottom part of the device. This feature would reduce a lot the workspace of a 7 DoFs system in the case of the user is a seated position since the wrist module can hit the legs. The mass distribution of the solution reported in Fig. 2e limits the use of that device to grounded applications. Finally, even if the solution shown in Fig. 2f is already a module of an upper limb exoskeleton and has a mass distribution that would allow a safe fine bimanual tasks, it cannot accommodate the hand exoskeleton due to the overall structure bulk.

III. WRIST INTERFACE DESIGN

The WRist ExoSkeleton (WRES) is a purely rotational 3 DoF forearm-wrist exoskeleton based on serial kinematics (shown in Fig. 3 and in Fig. 4), and powered by BLDC gearmotors. The device is able to elicit torques on the users' articulations: forearm pronation/supination (PS), wrist flexion/extension (FE) and radial/ulnar deviation (RU).

A. Requirements

The evidence that FE occurs slightly more proximal than RU ([14], [15], [16]), makes the wrist joint can be described kinematically as a universal joint with non-intersecting axes. Actually, the design process of the majority of the wrist exoskeletons ([11], [17], [9]) considered the wrist articulations to intersect in a point.

In order to develop ergonomically sound design, an exoskeleton system must conform to natural movements and limitations of a upper human limb. In fact, wrist articulations help the human perform complex motions of the hand. On the other side, the strict requirements about the compactness and the lightness unavoidably induced us to adopt the simplified model for the human wrist based on the spherical 3 DoFs kinematic chain. Hence, the orientation of the hand with respect to the arm can be studied in the 3-dimensional manifold SO(3).

Several studies have been carried on in providing normal standards for the functional range of motion (RoM) of the wrist during typical activities of daily living (ADL). In [18], a group of 40 healthy subjects was examined to define the ideal RoMs required to perform ADL, resulting in 40° for both dorsiflexion (or extension) and palmar flexion (or simply flexion), 30° of ulnar deviation, and 10° of radial deviation, which reflects the 70% wrist motion required for ADL. As reported in [19], the usual RoM for PS vary from 80° to 90° respectively. The magnitude of radial deviation reaches up to 25°, while ulnar deviation reaches the amplitude up to 45°, when the wrist is in the neutral location about FE. In its turn, FE motions have a range of up to 80° and 50° respectively, with the wrist in the neutral position about RU. The required torques for the ADL vary from 0.06 to 0.35 Nm, as reported in [6]. Further main requirements concern the lightness of the device, its easiness to be worn, and the need to have an open structure in order to allow the user to manipulate real objects or avoid collision between the upper bilateral arms exoskeleton ALEx, during bimanual operational task.

B. Kinematics & Mechanical design

The basic kinematics structure of WRES, depicted in Fig. 4a, is characterized by a spherical 3DoF kinematics based on serial configuration, that allows quasi-full RoM for the human wrist. A passive regulation of the handle position along the PS axis allows to adapt the last link length to the users hand size.

Serial kinematic configurations, compared to the parallel structure adopted in [11], [13], have the advantage not only to lead to simpler mechanical structures, but also to obtain a device ease to be worn by the user, or even better, by an impaired person involved in a robotic rehabilitation treatment. On the other side, the adoption of a cabled differential transmission allows the last two actuators to be fixed to the $link_1$ (moved by PS joint), while maintaining backlash-free, efficient and stiff

power transmission. Compared to a serial transmission, the differential solution simultaneously exploits the torque of both actuators for generating FE and RU joint torques, resulting in a higher torque/weight ratio. Concerning the inertia perceived by the user, the differential transmission results in a less pose dependent mass matrix, consequently reducing the effect of Coriolis and inertia disturbances during motions.

The WRES interface is a mechanically compliant robotic device, actuated by means of electric BLDC gearmotors with optical encoders. For WRES, the total weight is about 2.9 Kg including drivers box, of which about 1.8 Kg are due to the moving parts. Anodized aluminum alloy 7075-T6 has been used for most of the mechanical parts, due to its good tradeoff between high stiffness and lightness.

The PS joint has been designed to improve the wearability of the wrist device, by using an open curvilinear rail and rolling slider solution. Two $180 \deg$, 127mm diameter rail circular segments are mounted on both side of the moving cylindrical open hub. Two slider mechanisms, each mounted to a fixed frame, are used to support the required moment loads. The actuators 2 and 3 are remotely located with respect to the end-effector, both mounted on the link 1, in order to achieve the highest possible dynamic performances compatibly with a simple configuration for the cable routing of differential transmission.

The kinematics adopted in the last two DoF (RU and FE) of WRES combines the output motion of two parallel actuators by using a differential transmission, where the output, the joint variables q_2 and q_3, are given by the linear combination of the two motor variables, q_{m2} and q_{m3}, given by the relationship reported in the equation (1).

Fig. 5a shows a schematic representation of the transmission kinematics and the geometric notation adopted for its description. Both the motors act in parallel on the central main pulley through a double-stage pulley transmission each.

For compactness purpose and to make the structure open and easy to be worn by the user, two double-stage transmissions (named in Fig. 5a as cap_i and cap_e for the internal and external one, respectively) have been arranged on the same side, with respect to the $z_0 - z_2$ plane.

The first-stage pulley transmission for each motor is given through the capstans cap_{e1} and cap_{i1} (namely, driving capstans). The external capstan pair (red in Fig. 4c) is coupled through a hollow shaft, whereas the internal ones (green in Fig. 4c) are coupled rigidly. Both capstans, $2e$ and $2i$, drive directly the pulley of the link 3, and the link 2.

The 2 DoF, FE and RU, are actuated by means of the differential transmission, where the concurrent motion of both the capstan pairs cap_e and cap_i produces the rotation of link 2 and 3 around the horizontal axis z_1 (in Fig. 5c). The opposite motion of the capstan pairs produces a rotation of only the link 3 around the vertical axis z_2 (in Fig. 5b).

The relationships between joints and motor angles, due to the differential transmission, are given by the reduction matrix:

$$
\begin{bmatrix} q_1 \\ q_2 \\ q_3 \end{bmatrix} = \begin{bmatrix} 1/\tau_1 & 0 & 0 \\ 0 & -1/2\,\tau_2\,\tau_3 & -1/2\,\tau_2\,\tau_3 \\ 0 & 1/2\,\tau_2\,\tau_3 & -1/2\,\tau_2\,\tau_3 \end{bmatrix} \begin{bmatrix} q_{m1} \\ q_{m2} \\ q_{m3} \end{bmatrix} \quad (1)
$$

where $\tau_1 = R_1/R_m = 8.8$ represents the transmission ratios for the single-stage of capstan tendon transmission for PS joint ($R_1 = 88mm$ the PS capstan radius), $\tau_2 = R_p/R_{c2} = 1$, the second-stage of differential transmission and $\tau_3 = R_{c1}/R_m = 6.95$, the first-stage of differential transmission.

Given the equation (1), the positive direction of the joint q_2, reported in Fig. 5c, is given by the sum of negative contributions from both actuators, whereas the positive direction of the joint q_3 is given by the sum of the negative contribution from the actuator 3, and positive contribution from the actuator 2, as shown in Fig. 5b.

This kind of transmission makes the operation of device symmetric with respect to two possible motions of the hand exos (FE and RU joints), achieving high kinematic isotropy along these directions. As shown in Fig. 5, the torque transmission from the actuators to the FE and RU joints is achieved through in-tension stainless steel cables (1mm of diameter, 7x19 strand core) routed among drums, capstans and idle pulleys. Such a configuration allows for a high performance open loop force control without the use of costly force/torque sensors located at the end-effector of the manipulator or at its joints. The cables are pre-tensioned by using through-hole screws, and nuts are used to prevent cable loosening.

C. Technical specifications

The angular spatial resolution in the task space, related to the Jacobian matrix, is important to evaluate the haptic rendering resolution of the device. Angular rotations on the three gearmotor axes are acquired by means of 1024 quadrature-counts/revolution incremental optical encoders (Faulaber IER3-1024), resulting in a worst-case resolution of about $0.006°$ in the task space. The device is actuated by three BLDC gearmotors chosen to fit with the user requirements in providing haptic rendering, and to compensate for the weight and viscous friction of the device. In detail, gearmotor for the PS joint is composed of a 4 poles brushless DC servomotor (Faulhaber 3242G024BX4, max. continuous torque: 53 mNm, rated voltage: 24V) and a planetary gear head (Faulhaber 7 Nm 32/3S with two stages and reduction ration 14:1); the two gearmotors for the differential mechanism are identical and are composed of a 4 poles brushless DC servomotor (Faulhaber 2250S024BX4, max. cont. torque: 31.8 mNm, rated voltage: 24V) and a planetary gear head (Faulhaber 0.3 Nm 22/7 with one stage and reduction ration 3.71:1). The PS motor torque is significantly higher than the other two ones because it acts to move a larger inertia given by the rotating hub which support the last two motors and relative transmission stages.

The RoM of the three DoFs exceed or are slightly below the RoM of a healthy human wrist (see Table I) collected by averaging the data provided by several studies ([20], [21], [18], [22]), which carried on experimental evaluation of RoM of upper extremity joints during both simple active movements and most of ADLs, as reported in section III-A. The strict requirements about the reduced encumbrance inevitably has led to a reduced RoMs compared both to the other wrist devices and to the average values of ADLs RoM. Nevertheless,
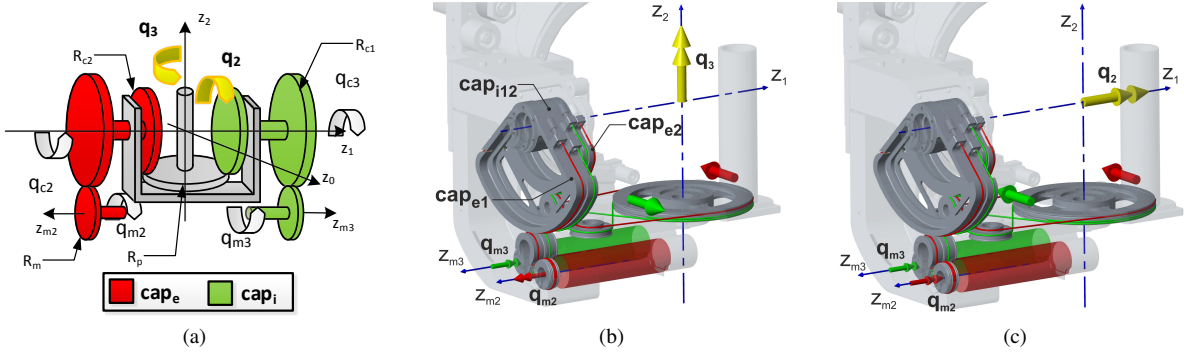
Fig. 5: The schematic representation of differential transmission kinematics and the main geometric parameters are reported in (a), where: $R_{c1} = 69.5mm$ the driving capstan radius, $R_{c2} = 46mm$ the driven capstan radius, $R_p = 46mm$ the differential pulley radius and $R_m = 10mm$ the motor drum radius. The two CAD model representations shows the cable routings for the motors 2 and 3. In (b) is shown the configuration for $q_{m2} = |q_m|$ and $q_{m3} = -|q_m|$, that results in $\boldsymbol{q_{FE}} = [0 \quad q_3]$, whereas in (c) for $q_{m2} = -|q_m|$ and $q_{m3} = -|q_m|$, we obtain $\boldsymbol{q_{RU}} = [q_2 \quad 0]$.

TABLE I: WRES capabilities compared with the requirements for ADL (the RoM data are averaged from [20], [21], [18], [6]; the torque data are from [6]) and the most recent wrist devices (IIT Wrist Device [9], WG [13], Open Wrist [12], RiceWrist-S [10], RiceWrist [11], CADEN7 [6]).

	ADL	WD	WG	OW	RW-S	RW-P	C7	**WRES**	ADL	WD	WG	OW	RW-S	RW-P	C7	**WRES**
Joint	[deg]				Range of Motion [deg]				[Nm]				Max Continuous Torque [Nm]			
PS	127.3	160	180	170	180	180	155	**146**	0.06	2.77	2.87	3.5	1.69	5.08	N.A.	**6.52**
FE	100.3	144	180	135	130	84	120	**75**	0.35	1.53	1.77	3.6	3.37	5.3	N.A.	**1.62**
RU	47.8	72	60	75	75	52	60	**40**	0.35	1.63	1.77	2.3	2.11	5.3	N.A.	**1.62**

the device is capable of spanning almost 115% of PS, 83% of RU and 75% of FE ROM during ADL. In terms of torque output capability, despite the requirement of compactness, thanks to the high torque/weight ratio (2.38 Nm/kg) and to the high torque/volume ratio ($0.87 \cdot 10^{-5}$ Nm/mm^3), the maximum continuous torques are 1.62 Nm both on FE and RU, and 6.52 Nm on PS, which are more than sufficient torque to replicate torques involved in ADL.

IV. ELECTRONICS AND CONTROL DESIGN

This section describes the control electronics and the control architecture of the wrist device.

A. Hardware setup

Each of the three BLDC gearmotors is controlled by a digital ethercat drive (Neptune Ingenia Drive) with a current control loop that runs at 10 kHz. The main control of the whole wrist device is executed on a generic personal computer with Simulink Real-Time running at 5 kHz.

B. Control scheme and gearmotor identification

The low-level control of the wrist exoskeleton takes into account two main feed-forward compensation terms: the gravity compensation and gearmotors viscous friction compensation. The viscous friction due to the transmission system has been neglected since all the pulleys and links are mounted on ball bearings. Fig. 6 shows the low-level control scheme where, τ_j^C and τ_m^C are the joint and motor control torques, τ_m^G and τ_m^V are the two motor torques to compensate the link weights and the

gearmotors unit viscous friction, τ_m^{drv} is the reference motor torque sent to the driver, θ_m and $\dot{\theta}_m$ are the motor position and speed, respectively. Finally, the τ_m^* takes into account the gearhead efficiency and it is computed as follow:

$$\tau_m^* = \begin{cases} \frac{\tau_m}{\eta_D}, & \text{if } \tau_m \dot{\theta}_m > 0 \\ \eta_I \tau_m, & \text{if } \tau_m \dot{\theta}_m < 0 \end{cases} \quad (2)$$

where $\eta_I = \frac{2\eta_D - 1}{\eta_D}$, η_D and η_I are the direct and indirect efficiencies of the gearhead. The analytic gravity compensation model of the moving links considers the device as a simple serial robot with three rotational joints also including the internal motion of the capstans. As above, the both direct and indirect gearhead efficiencies have been taken into account to compensate for the gearmotor behavior when it acts as motor or brake. In order to ascribe a physical meaning to each control block, a set of experiments has been conducted to independently identify the torque constant of the motors, the gearhead efficiency and the viscous friction of the gearmotors.
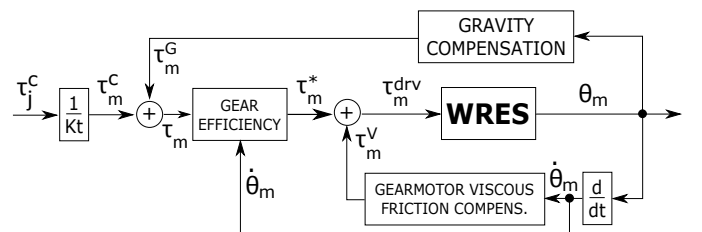

Fig. 6: **Low-level control scheme.**

As a first step, for torque constant identification, different loads have been applied on the gearmotor shaft by using a pulley. In detail, the motor current required for equilibrating the external loads has been recorded during the clockwise (CW) and counter-clockwise (CCW) slow rotations, hence against and in favor of the gravity. The motor torque constant, K_m, has been modeled as the slope of the curve obtained averaging the two load torque-current characteristics acquired during CW and CCW rotations (Fig. 7). Then, the direct gearhead efficiency has been computed by dividing K_m by the slope of the curve load torque-current acquired during the rotation made against gravity. As a second step, the estimated motor torque has been acquired at different motor speeds (both CC and CCW) without any load. The experimental torque-speed relation (that is the viscous friction) has been modeled as a simple multi-linear function (Fig. 7).

V. WRES EXPERIMENTAL EVALUATION

Two different experimental sessions have been performed: the first consisted in experimental measurements aiming to characterize bandwidth, and the static friction of each WRES joints. The resulting exoskeleton system was then evaluated by means of an haptic rendering application. The experimental application evaluated both system transparency in free movements and interaction with a virtual wall.

A set of experiments has been conducted to evaluate the performance of the proposed device. Firstly, the dynamic response of WRES has been evaluated. In detail, for each motor, a logarithmic chirp torque signal ranging from 1Hz to 80Hz has been fed to the motor driver. The result of the dynamic response of each gearmotor is reported in Fig. 8.

Static friction was then measured at each joint and at different joint angular positions. For each measurement, the joint was positioned using a closed-loop position control. Once the position of the joint was stabilized, the closed loop control was turned off and a feed-forward slow ramp (0.05 Nm/s at the joint) was fed as torque reference to the joint. The value of the torque was recorded when a displacement of 0.5 deg was recorded. Since gravity compensation was in force, for each measurement the test movement was operated twice in opposite directions and the value of the torque was averaged. Static friction measurements were performed on a set of eleven
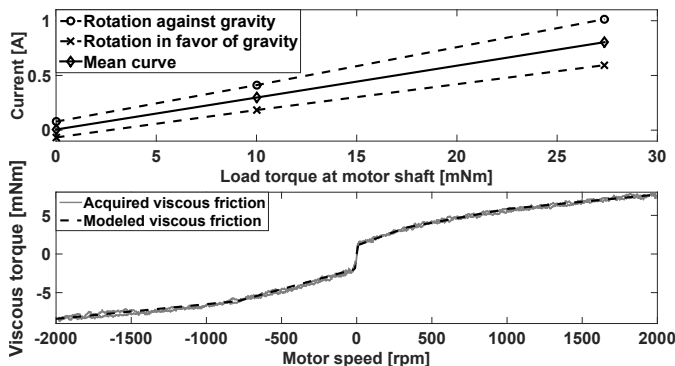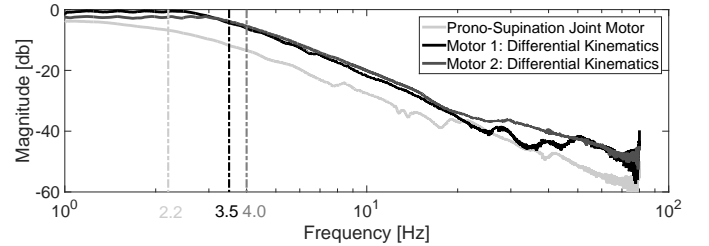

Fig. 8: **Dynamic Responses.** The magnitude (dB) of the transfer function $G(s) = \theta_m(s)/\tau_m(s)$ for each of the three gearmotors, where θ_m is the measured motor angle expressed in radians and τ_m is the estimated motor torque expressed in Nm. 2.2 Hz, 3.5 Hz and 4.0 Hz are the bandwith values individuated with the -3dB rule.

different joint angular positions, spanning the full range of each joint, and repeated five times for each position. Results of the static friction measurements are shown in Fig. 9. Following the experimental characterization of the system, we evaluated the transparency of the device, hence the accuracy of the feed-forward terms that are compensated into the low-level control: the gravity torque and the gearmotor viscous friction torque compensations. A six-axis force/torque sensor (ATI Gamma) was mounted at the base of the device handle to measure the interaction torques between the user and the haptic device. One subject was then asked to wear the wrist exoskeleton and perform several joint rotations, at different speeds, for each of the three joints. Fig. 10 reports the data acquired in this phase.

The WRES was finally implemented in a virtual haptic rendering application in order to validate the overall functionality of the system. As explained in the sketch in Fig. 11a, the haptic rendering application involved a virtual environment (VE) simulating interaction between a virtual stick held by the user's hand and a four walled box. Distance of the stick from the center of rotation of the wrist in the VE matched the real dimensions of the WRES handle (60 mm distance, 200 mm height of the tip). The stiffness and the viscous friction of the walls properties have been defined in the Cartesian space: the stiffness and viscous coefficient were set to 1.5 N/mm and 15 Ns/mm^2. The pose of the virtual stick has been computed by using the motor encoders data. Similarly to the previous experiment, interaction forces and torques between the WRES and the user were measured through the six axis force sensor

Fig. 7: **Joint 1 gearmotor data. (Top)** Currents-load torque curves. **(Below)** Experimental and modeled viscous friction.
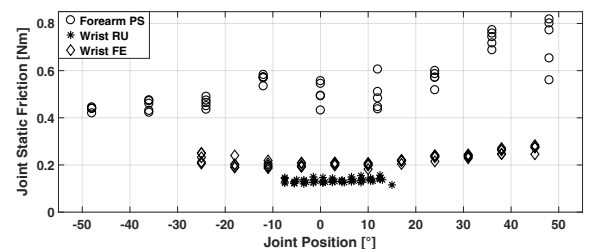

Fig. 9: **Static Friction.** Static friction measured for each joint and at different joint positions. Each point is the average of two test movements in opposite directions.
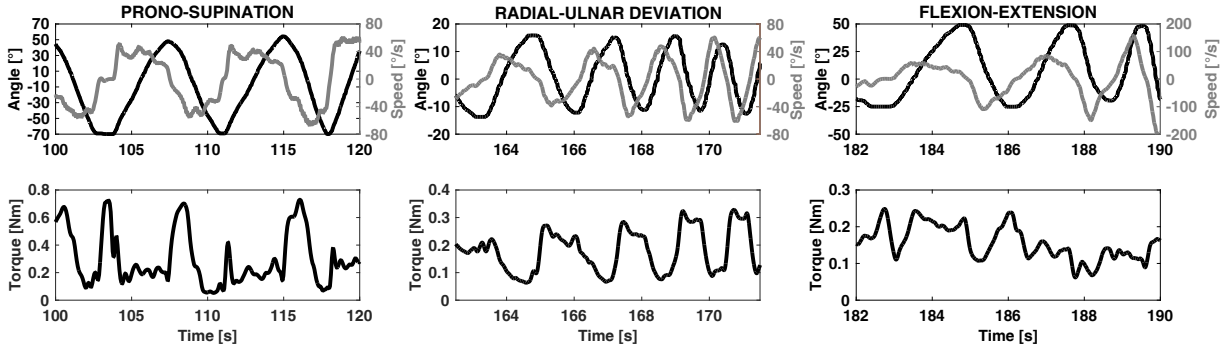
Fig. 10: **Transparency evaluation**. At the top row, the joint angle and speeds measured during the acquisition are reported for each of the three wrist joints. At the bottom row, the module of the total torque applied at wrist center of rotation.
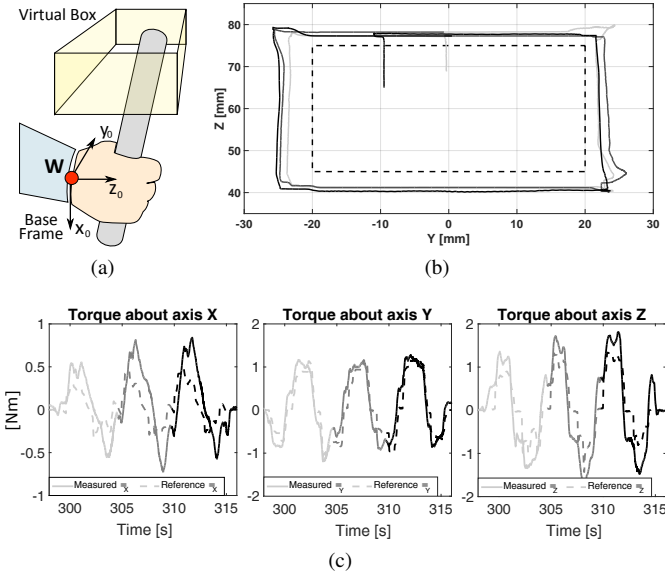

Fig. 11: **Haptic rendering.** (a) Scheme of the implemented haptic rendering application, involving interaction with virtual walls. (b) Position in the cartesian coordinates of the end effector (solid lines) interacting with virtual walls (dotted line) during exploration of the wall perimeter performed by a human user. (c) Measured interaction torques (solid lines) and reference torques (dotted lines) generated by the virtual wall in the base frame. Different grayscale colors indicate different loops of exploration of the box perimeter.

mounted at the handle (sensor was used just for measurement and did not fed any information to the WRES control). Fig. 11c shows results related to one subject exploring the boundaries of the virtual three times. Forces and torques measured by the force sensor, and reference forces generated by the virtual wall were both transposed to the three-dimensional space of the WRES base frame.

VI. DISCUSSION

Characterization of the WRES underscores the significance of the numerous design considerations. Considering the data reported in Table I it emerges that the WRES joint range of motions and maximum continuous torques are consistent with

the values required during the activities of daily living. This result indicates the device suitability in rehabilitation protocol. The main effect of the strict design requirements (see Sec.I and Sec.III-A) is the reduced RoMs compared to most recent devices (Table I). On the other hand, the compactness and the high torque/volume and torque/weight ratios ensure joint maximum continuous torques consistent with the averaged values of other devices.

Analyzing the results of the static friction identification and the transparency tests (Fig. 9), it can be stated that the final device has respected the requirement of being an impedance-type device. The FE joint showed lower friction than the RU joint (FE 0.133 ± 0.004 Nm, RU 0.223 ± 0.025), since it does not involve the internal movement of the differential mechanism as for the RU joint. Friction of the PS joint (0.572 ± 0.130 Nm), exhibits an increasing trend towards higher angular position of the PS joint: this trend is explained by the different direction of the gravity force and of the resulting momentum applied to the bearings of the circular guide. Unlike both the FE and RU joints, the PS static friction measurements present a higher variability due to the effect of the two stages high reduction gearhead. In Fig. 10 it is worth noticing that, although the joint speeds reached very high values (up to 60 deg/s for PS and RU joints and up to 200 deg/s for FE joint), the module of the interaction torque is less than 0.8 Nm for the PS joint, 0.3 Nm for the RU joint and 0.3 Nm for the FE joint. The PS presents higher interaction torque values over time; this feature is motivated by the higher inertia of the link 1 and the higher static friction of the PS joint as shown in Fig. 9.

Results in Fig. 11c show consistency of the whole system in the haptic rendering. Regarding performance of the haptic rendering, the RMSE between reference and measured torques at the base frame were: X: 0.270 Nm, Y: 0.271 Nm, Z: 0.500 Nm. The values of the measured RMSE errors of each axis are comparable with values of static friction measured in the previous experimental session. Static friction could not be compensated since the proposed solution does not use force/torque sensors able to measure the user interaction force: bottom graphs of Fig. 11c (in particular for axis X and Z) also show how error between the reference and the measured torque was higher in regions with higher interaction forces with the
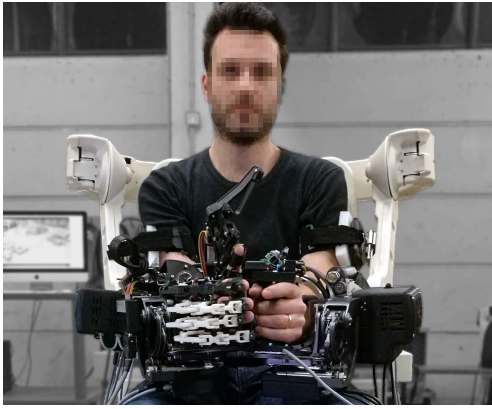
Fig. 12: Integration of WRES interface on ALEx.

virtual wall and lower velocities along the specific axis.

The wrist exoskeleton WRES has been integrated with the fully actuated four DoFs ALEx and the hand exoskeletons (Fig. 12). When the user wears both exoskeleton arms with two WRESs (both left and right versions), the experimental minimum distance between the two hand palms is 8 cm (measured for symmetric poses of the arms). Moreover, from the Fig. 12 it can be noted that the user wearing the full system would be able to put in contact the fingers of both hands, thus allowing bi-manual interaction even with small real or virtual objects.Finally, it is worth noting that, when WRES is used with the hand-exoskeleton (Fig. 12), the hand palm of the user is fixed through belts and a rigid support to the last link of the WRES in place of the handle.

VII. CONCLUSION

The WRES wrist exoskeleton meets the design goals needed for a fully actuated bimanual upper limb exoskeleton including a hand exoskeleton. Experimental tests demonstrated that the novel mechanical design balances the tradeoffs inherent in haptics and rehabilitation exoskeleton device design . The device is characterized by a spherical serial kinematics, based on tendon transmissions, and adopting a capstan-based tendon driven differential transmission. The proposed solution allows for a compact interface design, centered around the human wrist, matching the desired workspace specifications for all joints. Future works will focus on the system evaluation in fine manipulation bimanual tasks and on the improvement in the design, focusing on the weight reduction and a more ergonomics physical interface.

ACKNOWLEDGMENT

REFERENCES

[1] M. Bergamasco, A. Frisoli, and C. A. Avizzano, *Exoskeletons as Man-Machine Interface Systems for Teleoperation and Interaction in Virtual Environments*. Berlin, Heidelberg: Springer Berlin Heidelberg, 2007, pp. 61–76.

[2] L. Marchal-Crespo and D. J. Reinkensmeyer, "Review of control strategies for robotic movement training after neurologic injury," *Journal of neuroengineering and rehabilitation*, vol. 6, no. 1, p. 20, 2009.

[3] P. Maciejasz, J. Eschweiler, K. Gerlach-Hahn, A. Jansen-Troy, and S. Leonhardt, "A survey on robotic devices for upper limb rehabilitation," *Journal of neuroengineering and rehabilitation*, vol. 11, no. 1, p. 3, 2014.

[4] E. Pirondini, M. Coscia, S. Marcheschi, G. Roas, F. Salsedo, A. Frisoli, M. Bergamasco, and S. Micera, "Evaluation of the effects of the arm light exoskeleton on movement execution and muscle activities: a pilot study on healthy subjects," *Journal of neuroengineering and rehabilitation*, vol. 13, no. 1, p. 9, 2016.

[5] M. Sarac, M. Solazzi, D. Leonardis, E. Sotgiu, M. Bergamasco, and A. Frisoli, *Design of an Underactuated Hand Exoskeleton with Joint Estimation*. Springer International Publishing, 2017, pp. 97–105.

[6] J. C. Perry, J. Rosen, and S. Burns, "Upper-limb powered exoskeleton design," *IEEE/ASME transactions on mechatronics*, vol. 12, no. 4, pp. 408–417, 2007.

[7] T. Nef, M. Guidali, and R. Riener, "Armin iii–arm therapy exoskeleton with an ergonomic shoulder actuation," *Applied Bionics and Biomechanics*, vol. 6, no. 2, pp. 127–142, 2009.

[8] B. Kim and A. D. Deshpande, "An upper-body rehabilitation exoskeleton harmony with an anatomical shoulder mechanism: Design, modeling, control, and performance evaluation," *The International Journal of Robotics Research*, p. 0278364917706743, 2017.

[9] L. Cappello, N. Elangovan, S. Contu, S. Khosravani, J. Konczak, and L. Masia, "Robot-aided assessment of wrist proprioception," *Frontiers in Human Neuroscience*, vol. 9, p. 198, 2015.

[10] A. U. Pehlivan, F. Sergi, A. Erwin, N. Yozbatiran, G. E. Francisco, and M. K. O'Malley, "Design and validation of the ricewrist-s exoskeleton for robotic rehabilitation after incomplete spinal cord injury," *Robotica*, vol. 32, no. 8, p. 14151431, 2014.

[11] A. Gupta, M. K. O'Malley, V. Patoglu, and C. Burgar, "Design, control and performance of ricewrist: A force feedback wrist exoskeleton for rehabilitation and training," *The International Journal of Robotics Research*, vol. 27, no. 2, pp. 233–251, 2008.

[12] E. Pezent, C. G. Rose, A. D. Deshpande, and M. K. O'Malley, "Design and characterization of the openwrist: A robotic wrist exoskeleton for coordinated hand-wrist rehabilitation," in *2017 International Conference on Rehabilitation Robotics (ICORR)*, July 2017, pp. 720–725.

[13] J. A. Martinez, P. Ng, S. Lu, M. S. Campagna, and O. Celik, "Design of wrist gimbal: A forearm and wrist exoskeleton for stroke rehabilitation," in *2013 IEEE 13th International Conference on Rehabilitation Robotics (ICORR)*, June 2013, pp. 1–6.

[14] A. Goto, H. Moritomo, T. Murase, K. O. K. Sugamoto, T. Arimura, J. Masumoto, S. Tamura, H. Yoshikawa, and T. Ochi, "In vivo three-dimensional wrist motion analysis using magnetic resonance imaging and volume-based registration," *Journal of Orthopaedic Research*, vol. 23, 2005.

[15] R. A. Kaufmann, H. J. Pfaeffle, B. D. Blankenhorn, K. Stabile, D. Robertson, and R. Goitz, "Kinematics of the midcarpal and radiocarpal joint in flexion and extension: An in vitro study," *The Journal of Hand Surgery*, vol. 31, no. 7, pp. 1142–1148, 2006.

[16] S. K. Charles and N. Hogan, "Dynamics of wrist rotations," *Journal of Biomechanics*, vol. 44, no. 4, pp. 614 – 621, 2011.

[17] A. U. Pehlivan, S. Lee, and M. K. O'Malley, "Mechanical design of ricewrist-s: A forearm-wrist exoskeleton for stroke and spinal cord injury rehabilitation," in *2012 4th IEEE RAS EMBS International Conference on Biomedical Robotics and Biomechatronics (BioRob)*, Rome, Italy, June 2012, pp. 1573–1578.

[18] J. Ryu, W. P. Cooney, L. J. Askew, K.-N. An, and E. Y. Chao, "Functional ranges of motion of the wrist joint," *The Journal of Hand Surgery*, vol. 16, no. 3, pp. 409 – 419, 1991.

[19] Y. Youm and A. E. Flatt, "Design of a total wrist prosthesis," *Annals of biomedical engineering*, vol. 12, no. 3, pp. 247–262, 1984.

[20] D. H. Gates, L. S. Walters, J. Cowley, J. M. Wilken, and L. Resnik, "Range of motion requirements for upper-limb activities of daily living," *Am J Occup Ther*, vol. 70, no. 1, Dec 2016, 015487[PII].

[21] J. Aizawa, T. Masuda, T. Hyodo, T. Jinno, K. Yagishita, K. Nakamaru, T. Koyama, and S. Morita, "Ranges of active joint motion for the shoulder, elbow, and wrist in healthy adults," *Disability and Rehabilitation*, vol. 35, no. 16, pp. 1342–1349, 2013, pMID: 23826904.

[22] J. Rosen, J. C. Perry, N. Manning, S. Burns, and B. Hannaford, "The human arm kinematics and dynamics during daily activities - toward a 7 dof upper limb powered exoskeleton," in *ICAR '05. Proceedings., 12th International Conference on Advanced Robotics, 2005.*, July 2005, pp. 532–539.